International Journal of Neural Systems, Vol. 17, No. 4 (2007) 231–240

World Scientific
www.worldscientific.com

A MODEL OF GRID CELLS BASED ON A TWISTED TORUS TOPOLOGY

ALEXIS GUANELLA* and DANIEL KIPER†
Institute of Neuroinformatics, Swiss Federal Institute of Technology (ETH), 190 Winterthurerstrasse, 8057 Zürich, Switzerland
**guanella@ini.phys.ethz.ch*
†*kiper@ini.phys.ethz.ch*

PAUL VERSCHURE
ICREA & Institute of Audio-Visual Studies, University Pompeu Fabra, Ocata 1, 08003 Barcelona, Spain
paul.verschure@upf.edu

The grid cells of the rat medial entorhinal cortex (MEC) show an increased firing frequency when the position of the animal correlates with multiple regions of the environment that are arranged in regular triangular grids. Here, we describe an artificial neural network based on a twisted torus topology, which allows for the generation of regular triangular grids. The association of the activity of pre-defined hippocampal place cells with entorhinal grid cells allows for a highly robust-to-noise calibration mechanism, suggesting a role for the hippocampal back-projections to the entorhinal cortex.

Keywords: Grid cells; place cells; entorhinal cortex; path integration; twisted torus.

1. Introduction

The grid cells of the rat medial entorhinal cortex (MEC) show an increased firing frequency when the position of the animal correlates with multiple regions in an environment, or subfields, that are arranged in regular triangular grids.[1–3] These grids can be characterized by only a few parameters: their orientation, phase and spacing (i.e. the minimal inter-subfield distance). With these parameters, it has been shown that grid cells are topographically organized in the MEC: first, neighboring cells share common grid orientation and spacing; second, the grid spacing isometrically increases along the dorsoventral axis (in Ref. 1, the grid spacing varies between 39 to 73 cm).

It has been proposed that grid cells may be part of a generalized path integration system.[1,4,5] Three main arguments confirm this hypothesis: first, entorhinal lesions disrupt the return path that rats follow;[6] second and third — which also suggests hard wired connections — the grid structure is expressed instantaneously in novel environments[1] and the spacing parameter does not depend on allothetic (external) information (for instance, the grid spacing remains constant when the size of the arena is increased[1]). This raises the question of how such a system can be implemented in the brain. In addition, since a path integration system is inherently prone to the accumulation of errors, it remains to be determined how the grids can be anchored to allothetic information.

In this study, we first describe an artificial neural network that implements grid cells as a path integration mechanism. In this model, the activity of rate coded neurons is transduced and shifted by asymmetric synaptic connections. These connections are modulated by the velocity of the animal that is represented by a virtual rat exploring randomly a square arena. The network connectivity, which is organized cyclically, can be represented by a twisted torus. This topology allows for the generation of regular triangular grids sharing the same orientation and spacing,

but different phases, as neighboring MEC grid cells. Second, we describe an associative system that calibrates the grids using allothetic information. We generate the neural activity of a population of hippocampal place cells[7] that code for unique regions in an environment. We connect these place cells as input to the population of grid cells using a Hebbian associative learning rule, combining the idiothetic (internal) representations of grid cells with this allothetic information. In this way, the model grid cells are permanently recalibrated using the set of hippocampal place cells, allowing for the correction of large path integration errors. Even if nothing is initially known about the phase, orientation and spacing of the grids, the grid cell mean activity maps are intrinsically learned in the synaptic weights connecting place cells to grid cells. As a result, a coherent representation of space is constructed.

2. Methods

2.1. *Model of grid cells*

2.1.1. *Virtual rat and environment*

We simulated a virtual rat exploring a $1 \times 1\,\mathrm{m}^2$ arena. The movements of the virtual rat alternated randomly (at each time step with a probability of 0.5) between translations (maximum 2.75 cm/time step) and rotations (maximum $\frac{\pi}{10}$ rad/time step), that were combined with obstacle avoidance at the walls based on a reactive Braitenberg neural controller.[8]

2.1.2. *Grid cell sheet*

We constructed a population of $N = N_x \times N_y$ or 10×9 neurons organized in a matrix (or grid cell sheet) covering the repetitive rectangular structure formed by the grid subfields (Fig. 1a). To conserve the ratio between the height and the side of an equilateral triangle (which is the core element of a regular triangular tessellation) and to allow for the same density of cells along both x- and y-axes, the number of cells in each row was chosen to be approximately $2/\sqrt{3}$ times larger than the number of cells in each column (Fig. 1b).

2.1.3. *Grid cell sheet synapses*

The synapses of the grid cell sheet can be divided into two distinct populations. The first population is formed by the synapses that are used to compute the overall neural activity of the sheet and to stabilize it. They connect all the sheet cells to an external cell $N+1$ that computes the sum of all activities. These synapses have constant synaptic weights that are all set to 1. The second population is formed by the synapses implementing attractor dynamics on the

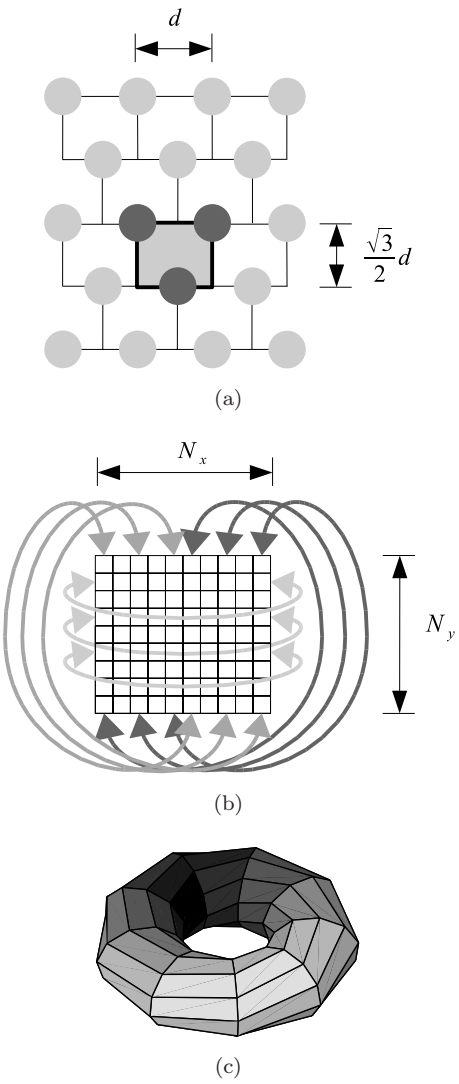

Fig. 1. (a) Repetitive rectangular structure (gray filled rectangle) of the grid subfields (gray circles), which define a regular triangular tessellation of space. d represents the minimal distance between two subfields, i.e. the grid spacing. (b) Matrix of a population of 10×9 grid cells (grid cell sheet). Neighboring relationships between cells on the side of the structure are represented by gray arrows. For instance, neurons at two opposite vertical sides are neighbors. (c) Representation of the grid cell sheet on a twisted torus, with one locus of activity over the cell population: dark regions and light regions represent high and low cell activity respectively.

grid cell sheet. They connect each cell i to each cell j, with $i, j \in \{1, 2, \ldots, N\}$. The synaptic weights are computed as a Gaussian function of a toral distance between cells (exciting neighboring and inhibiting distal cells, Fig. 2a and Eq. 3) to maintain a single locus of activity over the grid cell sheet. In addition, these connections are modulated by the speed of the virtual rat, which allows shifting the locus of activity in a manner consistent with the rat's motion.

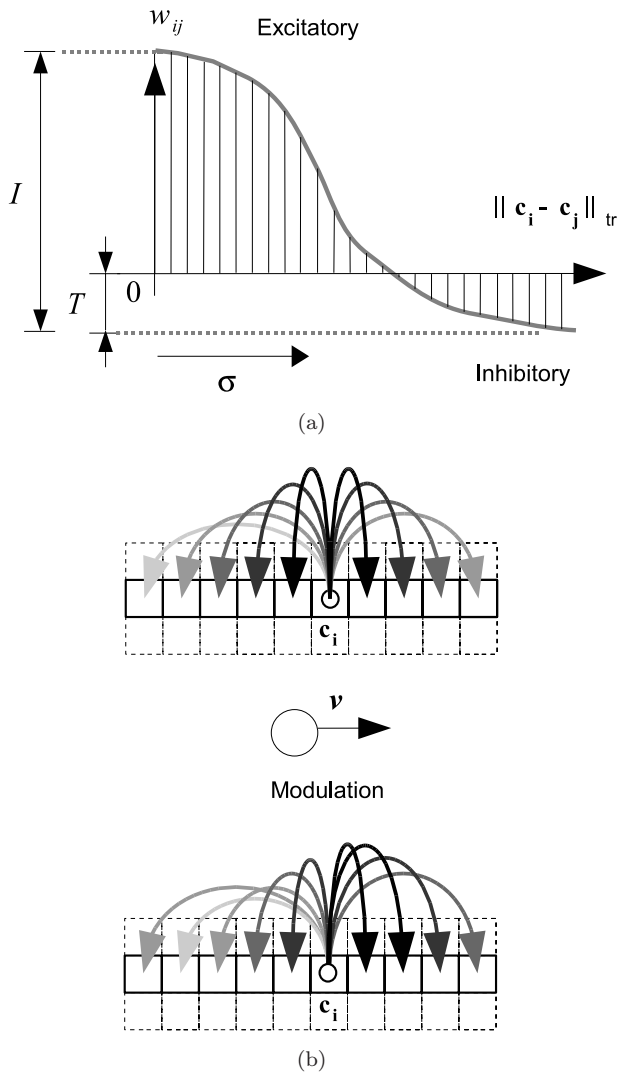

Fig. 2. (a) Synaptic weights connecting cell i to other grid cells. Intensity, shift and width parameters are represented by I, T and σ respectively, defining excitatory and inhibitory connections. $\| \mathbf{c_i} - \mathbf{c_j} \|_{tri}$ represents the toral distance between cells i and j. (b) Modulation of the synaptic connections of a cell i. Before modulation, the synaptic pattern of the cell is centered around $\mathbf{c_i}$. After modulation, the synaptic pattern is shifted in the direction of the speed $\mathbf{v}$ of the virtual rat, leading to an asymmetric synaptic pattern. Dark and light arrows represent high and low synaptic connections respectively. For simplicity, only the synaptic weights along an horizontal axis are represented.

2.1.4. *Activity and stabilization*

The neurons of the grid cell sheet are initialized with a random activity that is uniformly distributed between 0 and $1/\sqrt{N}$. The activity of a cell j at time $t+1$, i.e. $A_j(t+1)$ is defined using a linear transfer function $B_j(t+1)$ given by

$$B_j(t+1) = \sum_{i=1}^{N} A_i(t)\, w_{ij}(t), \tag{1}$$

where $w_{ij}(t)$ is the synaptic weight connecting cell i to cell j, with $i, j \in \{1, 2, \ldots, N\}$. A floating normalization mechanism over the cell activity ensures the stability of the network:

$$A_j(t+1) = (1-\tau)B_j(t+1) + \tau \left(\frac{B_j(t+1)}{\sum_{i=1}^{N} A_i(t)} \right), \tag{2}$$

where $\sum_{i=1}^{N} A_i(t)$ is computed locally using the activity of external cell $N+1$ and where the parameter τ determines the stabilization strength. In order to prevent negative cell activities, we set $A_j(t+1) = 0$ when $A_j(t+1)$ is smaller than zero.

2.1.5. *Attractor dynamics*

The Gaussian weight function defining the synaptic patterns connecting the neurons of the grid cell sheet is given by

$$w_{ij} = I \exp\left(-\frac{\| \mathbf{c_i} - \mathbf{c_j} \|_{tri}^2}{\sigma^2} \right) - T, \tag{3}$$

where $\mathbf{c_i} = (c_{i_x}, c_{i_y})$ is the position of the cell i on the sheet, defined by $c_{i_x} = (i_x - 0.5)/N_x$ and by $c_{i_y} = \frac{\sqrt{3}}{2}(i_y - 0.5)/N_y$ respectively (with $i_x \in \{1, 2, \ldots, N_x\}$ and $i_y \in \{1, 2, \ldots, N_y\}$) and where i_x and i_y are the column and the row number of cell i. I is the intensity parameter, defining the overall synaptic strength, σ regulates the size of the Gaussian and T is the shift parameter determining excitatory and inhibitory connections (Fig. 2a). The norm $\| \cdot \|_{tri}$ defines the induced metric $\mathrm{dist}_{tri}(.,.)$ of the network. To obtain the repetitive rectangular structure of the grid subfields (Fig. 1a), the cells at the border of the layer have to be the neighbors of the

cells at the opposite border (Fig. 1b). This structure is equivalent to a torus. However a simple torus is not sufficient, since it would lead to regular rectangular tessellations. The regular triangular tessellation is generated by twisting the torus (Fig. 1c), which is implemented in the definition of the distance $\mathrm{dist}_{tri}(.,.)$ or the norm $\| \cdot \|_{tri}$:

$$\begin{aligned} \mathrm{dist}_{tri}(\mathbf{c_i}, \mathbf{c_j}) &:= \| \mathbf{c_i} - \mathbf{c_j} \|_{tri} \\ &= \min_{j=1}^{7} \| \mathbf{c_i} - \mathbf{c_j} + \mathbf{s_j} \|, \end{aligned} \tag{4}$$

where

$$\begin{aligned} \mathbf{s_1} &:= (0,0), \\ \mathbf{s_2} &:= \left(-0.5, \frac{\sqrt{3}}{2}\right), \\ \mathbf{s_3} &:= \left(-0.5, -\frac{\sqrt{3}}{2}\right), \\ \mathbf{s_4} &:= \left(0.5, \frac{\sqrt{3}}{2}\right), \\ \mathbf{s_5} &:= \left(0.5, -\frac{\sqrt{3}}{2}\right), \\ \mathbf{s_6} &:= (-1,0), \\ \mathbf{s_7} &:= (1,0), \end{aligned} \tag{5}$$

and where $\| \cdot \|$ is the Euclidean norm.

2.1.6. *Modulation*

The main input of the network is the speed vector $\mathbf{v} := (v_x, v_y)$, which represents the speed of the virtual rat. This input does not depend on any absolute information about the location of the animal. The maximum velocity of the virtual rat is determined by the parameter v_{max} such that $\|\mathbf{v}\|$ is always smaller than v_{max}.

It is possible to increase or decrease the size and the spacing of the grid subfields, as well as to rotate the grid, by changing only two parameters in the model: the gain $\alpha \in \mathbb{R}_+$ and the bias $\beta \in [0, \pi/3]$. The input of the network is thus modulated and biased by the gain and bias parameters, with

$$\mathbf{v} \mapsto \alpha \, \mathbf{R}_\beta \mathbf{v}, \tag{6}$$

where $\mathbf{R}_\beta$ is the rotation matrix of angle β defined by

$$\mathbf{R}_\beta = \begin{pmatrix} \cos(\beta) & -\sin(\beta) \\ \sin(\beta) & \cos(\beta) \end{pmatrix}. \tag{7}$$

The activity pattern of the grid cell sheet is stable when the virtual rat stays put. However, when the rat moves, the synaptic connections of the network shift it in the direction of the speed vector of the virtual rat (Fig. 2b). When expressing the synaptic weight as a function of time we have

$$w_{ij}(t) = I \exp\left(-\frac{\| \mathbf{c_i} - \mathbf{c_j} + \alpha \, \mathbf{R}_\beta \, \mathbf{v}(t) \|^2_{tri}}{\sigma^2}\right) - T. \tag{8}$$

2.2. *Calibration mechanism*

2.2.1. *Noise and idiothetic error*

To test the stability of the model to noisy inputs, we added white noise to the idiothetic information (i.e. the speed vector $\mathbf{v}$). This noise is described by two independent uniform random variables $X, Y \sim \mathcal{U}(-\mu, \mu)$, where $\mu > 0$ is a scaling parameter for this distribution. The idiothetic estimation value $\widehat{\mathbf{v}}$ of the speed $\mathbf{v}$ is given by

$$\widehat{v_x} = v_x + X \parallel v_x \parallel, \tag{9}$$

and

$$\widehat{v_y} = v_y + Y \parallel v_y \parallel . \tag{10}$$

Unless stated otherwise, we used in the calibration experiments a value of $\mu = 0.5$, which corresponds to a noise level of 50% of speed of the virtal rat. Representative errors of path integration with this noise value are shown in Fig. 3.

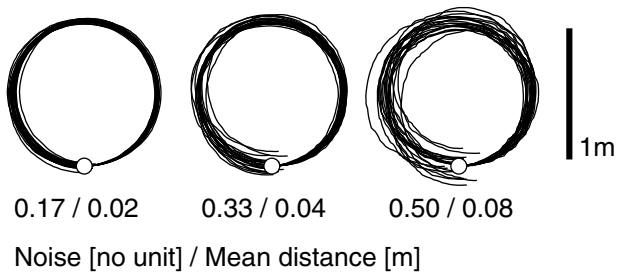

Fig. 3. 20 representative trajectories of the virtual rat with different levels of error in path integration. The rat moves around an imaginary circle of 1 m diameter. A white circle indicates the path start. A mismatch occurs between the initial position and the end position, due to the accumulation of path integration error, as indicated by the value of the mean distance between the starting and end position under the plots.

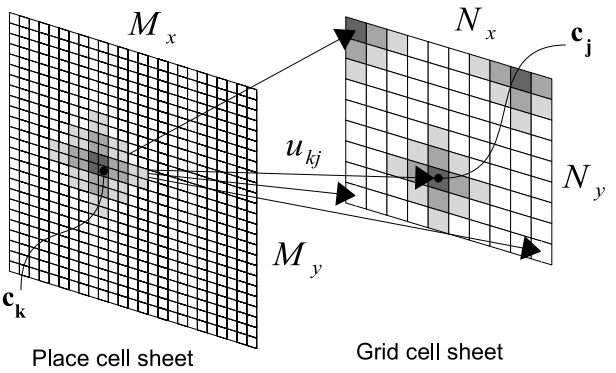

Fig. 4. A population of 25×25 place cells, driven by allothetic inputs, is connected to the population of entorhinal grid cells. M_x, M_y, N_x and N_y indicate the number of columns and rows on the place and grid cell sheets respectively. u_{kj} represents the synaptic weight between cell k and j, and $\mathbf{c}_k, \mathbf{c}_j$ indicate the respective cell positions.

2.2.2. *Place cell sheet*

We constructed a place cell sheet of $M = M_x \times M_y = 25 \times 25$ neurons (Fig. 4) using the model proposed in Ref. 9, i.e. formed by the thresholded sum of Gaussian tuning curves each oriented perpendicular to the walls of the environment. This model, which explains how place fields can expand when the size of the environment is increased, provides a good approximation of the place fields observed in the rat. It has also been generalized to a model that supports real-world robot navigation.[10] Moreover, we have previously shown how these place fields, that are view dependent representations of visual stimuli, can be generated by a real-world visual system.[11] We can thus refer to these inputs as allothetic information.

The activity C_k of a place cell k is defined by

$$C_k(\mathbf{x}) = \exp\left(-\frac{\| \mathbf{x} - \mathbf{d_k} \|^2}{\gamma^2}\right), \tag{11}$$

where $\mathbf{x}$ is the position of the virtual rat and $\mathbf{d_k} = (d_{k_x}, d_{k_y})$ is the position of cell k on the place cell sheet, defined by $d_{k_x} = (k_x - 0.5)/M_x$ and $d_{k_y} = (k_y - 0.5)/M_y$ respectively and where k_x and k_y are the column and the row numbers. γ is chosen such that place fields slightly overlap their neighbors ($\gamma = 0.1$) .

2.2.3. *Synaptic connections from place cells to grid cells*

Each place cell is connected to each grid cell (Fig. 4). Grid cells and place cells are correctly associated when each place cell, coding for a unique region in the environment, is combined with the grid cells that have a subfield at approximately the same region. Hebbian synapses are well suited to learn these associations, since they strengthen connections between neurons with correlated activity. In the case of a path integration error, the place cell input may not match anymore the position of the locus of activity on the grid cell sheet. However, because of the attractor dynamics of the grid cell matrix, the locus of activity will return to its correct position, attracted back by the learned associated input provided by the place cells, which is projected to the grid cell sheet.

To stabilize these synaptic weights, which would be growing infinitely since pre- and postsynaptic activities are both positive by definition, we additionally used Oja's learning rule.[12] To satisfy the biological constraint of locality we restricted it to its first order terms in the learning rate η,[13] assumed to be small. Therefore, a synapse u_{kj} that connects an afferent neuron k (place cell) to an efferent neuron j (grid cell) is updated as follows:

$$u_{kj}(t+1) = \begin{cases} u_{kj}(t) + \eta \ \triangle A_j(t)(\triangle C_k(t) - \ \triangle A_j(t) u_{kj}(t)) \\ \qquad \text{if } \triangle A_j(t) > 0 \text{ or } \quad \triangle C_k(t) > 0, \\ u_{kj}(t) \quad \text{else.} \end{cases} \tag{12}$$

where $\triangle A_j(t) = A_j(t) - \langle A_i(t-1) \rangle_{i=1}^N$ and $\triangle C_k(t) = C_k(t) - \langle C_l(t-1) \rangle_{l=1}^M$ and where C_k is the activity of the presynaptic cell k and A_j the activity of the postsynaptic cell j. The function $\langle \cdot \rangle$ is the mean over the cells of a cell sheet (i.e. for instance $\langle A_i(t-1) \rangle_{i=1}^N = \sum_{i=1}^N A_i(t-1)/N$, which can be computed locally using the activity of the external cell $N+1$).

2.2.4. *Updating process*

At each time step, the population activity of the place cell sheet is integrated by each grid cell j. Thus, using Eq. 2, we now have

$$A_j(t+1) = (1-\tau) B_j(t+1) + \tau \left(\frac{B_j(t+1)}{\sum_{i=1}^N A_i(t)} \right) + \lambda \sum_{k=1}^M C_k(t) u_{kj}(t), \tag{13}$$

where λ determines the strength of the place cell input.

2.2.5. *Correlation between the mean activity maps of grid cells and the synaptic patterns connecting place cells to grid cells*

To compute the mean activity map of a grid cell j, we discretized the environment into 40×40 bins. We measured the mean activity of the cell in each bin, and divided this value by the number of time it was visited by the rat. To compute the correlation between the mean activity map of a grid cell and the synaptic connections connecting the place cell sheet to this grid cell, we constructed a similar mean activity map, but with 25×25 bins, corresponding to the number of place cells.

The correlation was then computed using this mean activity map and the synaptic weight matrix $U = (u_{kj})$ where $k \in \{1, 2, \ldots, M\}$ and $j \in \{1, 2, \ldots, N\}$.

2.3. *Parameters*

The values of the parameters used in this study are given in Table 1. These values have to satisfy two criteria. First, they have to ensure the stability of the cells of the network. This means for instance that the cell activity should not increase without bound. Second, they must induce the attractor dynamics of the grid cell sheet and therefore a single and stable locus of activity should be continuously observed in this population. Since no objective or cost function is given in this study, no parameter search was performed.

Table 1. Parameter values used in this study.

Parameter		Value	Unit
α	$\in$	$[1, 3]$	[no unit]
β	$\in$	$[0, \pi/3]$	[no unit]
μ	$\in$	$[0, 1]$	[no unit]
N	$=$	90	[cell]
N_x	$=$	10	[cell]
N_y	$=$	9	[cell]
τ	$=$	0.8	[no unit]
I	$=$	0.3	[no unit]
σ	$=$	0.24	[meter]
T	$=$	0.05	[no unit]
v_{max}	$=$	0.0275	[meter/time step]
M	$=$	625	[cell]
M_x	$=$	25	[cell]
M_y	$=$	25	[cell]
γ	$=$	0.1	[meter]
η	$=$	0.005	[no unit]
λ	$=$	0.01	[no unit]

3. Results

3.1. *Regular triangular tessellations*

To analyze the activity of the model grid cells, we first computed their mean activity maps, i.e. the mean activity of a cell as a function of the virtual rat's position. These maps showed a stable activity at multiple regions of the environment (Fig. 5). To determine whether these regions were organized in regular triangular tessellations, we fitted the mean activity maps to regular triangular tessellations composed of Gaussian subfields. The maps were normalized such that the maximum and the minimum intensity were 1 and 0 respectively.

We computed the mean square residuals over all the network cells, and found a mean square residual value of 0.0028 ± 0.0004 (mean $\pm$ s.d.), indicating the correct organization of the activity regions in regular triangular grids. For each cell this value was always smaller than 0.005. The stability of these patterns was confirmed by running the experiments over an extended number of time steps (1 million, data not shown).

3.2. *Gain and bias*

An interesting feature of our model is the possibility to vary the spacing and the orientation of the grids by just changing the gain and bias parameters. As shown in Figs. 5 and 6, higher gain values lead to denser grids (and therefore smaller grid spacing) whereas higher bias values rotate the grids. We performed a regression analysis to determine the relationship between the gain (respectively bias) parameter and the grid spacing (resp. orientation). For the gain, we found a logarithmic relationship, i.e. $y = a + b \log_2(x)$ where $a = 1.02$ and $b = -0.42$, with mean least square residuals of 0.00007 and where x and y are respectively gain and grid spacing. For the bias, we found a linear relationship, i.e. $y = a + bx$ where $a = 0.00$ and $b = 1.00$, with mean least square residuals of 0.00004 and where x and y are respectively bias and grid orientation.

3.3. *Calibration*

The addition of noise in the idiothetic inputs without calibration disrupted the organization of the

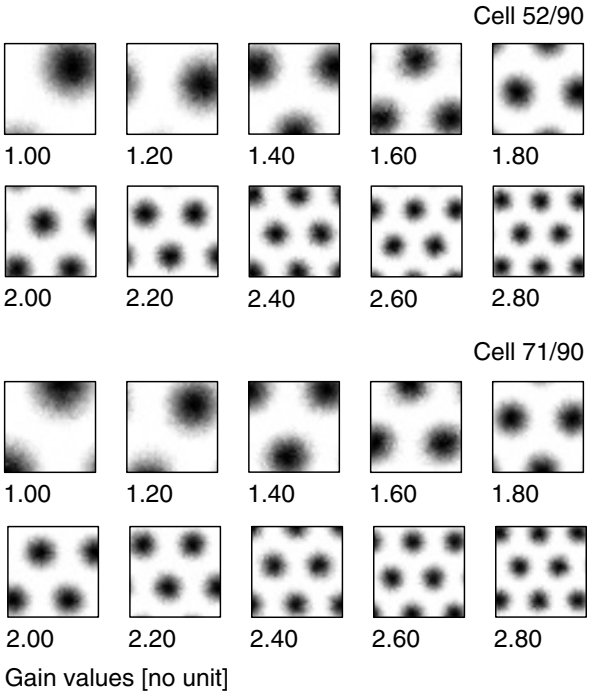

(a)

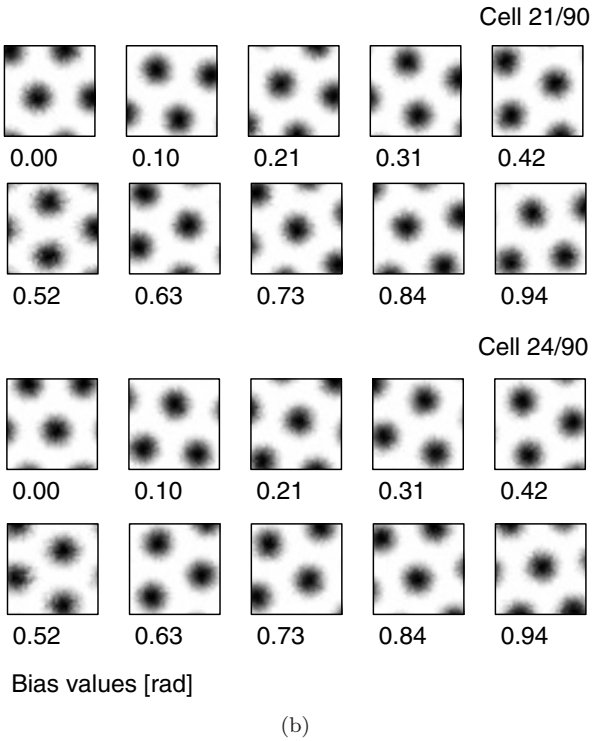

(b)

Fig. 5. (a) Mean activity maps of two grid cells with different gain values (here, the bias value is set to zero). Dark and light regions represent high and low mean activity respectively. These maps were computed over 50000 time steps. (b) Mean activity maps of two grid cells with different bias values (here, the gain value is set to 2).

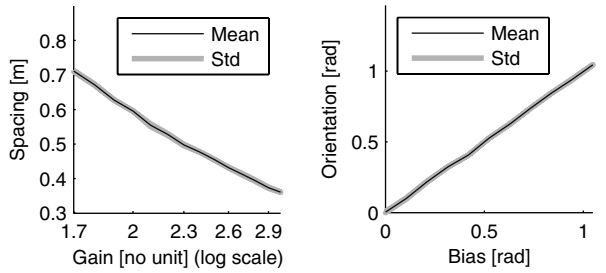

(a) (b)

Fig. 6. (a) Spacing of the grid as a function of the gain parameter. (b) Orientation of the grid as a function of the bias parameter.

subfields in regular triangular grids (Fig. 7b, without calibration). However, when the calibration mechanism was activated, we could again observe the characteristic mean activity maps of grid cells (Fig. 7b, with calibration). Hence the place cell input that was associated with the grids was fully correcting the errors of path integration.

Interestingly, we observed that the synaptic weights of the model were intrinsically coding for the grid cell mean activity maps (Fig. 7). We computed the median correlation between the grid mean activity maps and the synaptic weights of the network to determine their similarity. For this experiment, we used noise, gain and bias values of respectively $0.5, 2.3$ and 0. After growing very fast in the first 2K time steps, the median correlation slowly stabilized after about 6K time steps at a value of 0.84 ± 0.04 (mean$\pm$s.d.), ensuring that the grid patterns remain stable over time. In fact, a shifting of the grids would produce a mismatch between the grid cells and their associated place cells, leading to a decrease of the correlation between the grids and the synaptic weights. As observed in the dynamics of the synaptic patterns (Fig. 7b), the network associates place cells with a first grid subfield very early in the learning process. Subsequently, the positions of other subfields are learned, which increases the correlation between the grid mean activity maps and the synaptic weights (Fig. 7a).

To determine whether the system remains stable with higher noise values, we increased progressively the value of the noise parameter μ. We observed that even high path integration errors were corrected by the system, and, in particular, that the synaptic patterns remained correlated with the mean activity

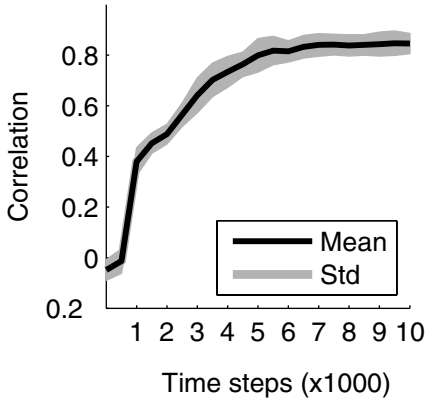

(a)

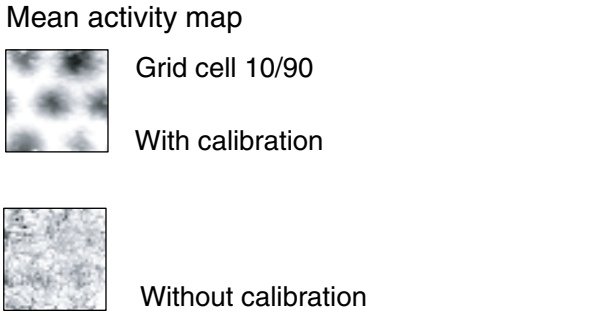

(b)

Fig. 7. Correlation between the synaptic weights connecting place cells to grid cells and the grid cell mean activity maps. For this experiment, gain, bias and noise values were set to 2, zero and 0.5 respectively. (a) Correlation as a function of the learning time. (b) *First row*: mean activity map of a representative grid cell (with added noise, *left*: with, *right:* without calibration). *Second row*: Synaptic weight patterns connecting the place cell population to this grid cell (each square represents a snapshot taken at a specific learning time indicated under the plot).

maps at higher noise values (Fig. 8). For noise values higher than 1, the calibration could not anymore correct these errors, and no triangular structure could be observed in the grid cell mean activity maps.

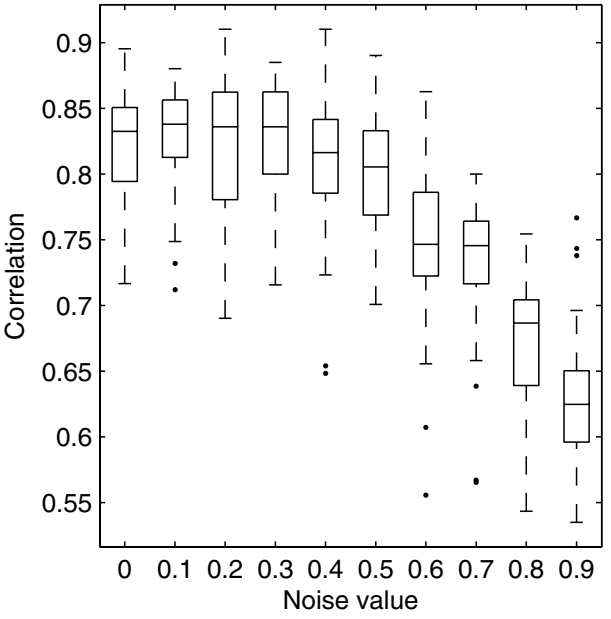

Fig. 8. Correlation between the synaptic weights and the mean grid cell activity maps as a function of the path integration error. The boxes have horizontal lines at the lower quartile, median, and upper quartiles. Whiskers show the extent of the rest of the data, black dots depict outliers.

4. Discussion

In this article, we have addressed the question of how grid cells can be generated in the MEC and how their activity can be calibrated against accumulated errors of path integration. We have presented a model of grid cells based on a twisted torus topology that generates regular triangular tessellations, as observed in MEC grid cells. In this model, the grids share the same orientation and spacing as observed in physiological recordings of neighboring MEC grid cells. We showed that a simple gain and bias mechanism can control in a log-linear and linear relationship the grid spacing and orientation respectively. Thus our model provides a parsimonious explanation of how cortical circuits can give rise to grid cells with different spacings and orientations using a single algorithm. In the MEC, the spacing of the grid isometrically increases along the dorsoventral axis.[1] Our model predicts that this effect is due to an exponential increase of the velocity gain along this axis.

Many studies present the implementation of path integration mechanisms based on attractor dynamics.[14–17] The idea to apply these methods to grid cells was first presented in Ref. 1 and described

further in Ref. 4. It has been implemented in Ref. 18, as a symmetric locally connected neural network. We provided the first model of such a system that is explicitly described and implemented on a cyclically connected map.[19] We have shown that this synaptic architecture that can be represented by a twisted torus generates regular triangular tessellating patterns. The advantages of our model is that it allows implementing a representation of space covering large environments using a relatively small population of cells. Moreover, because of this particular circular synaptic connectivity, all network cells have regular triangular tessellating subfields.

Our model of grid cells may be used as the proprioceptive element of a robust, modulatory and biologically based navigational system combining idiothetic and allothetic information. The classic problem of purely allothetic systems is their inability to disambiguate between two similar inputs. For instance, realistic models of place cells of the hippocampus, based on visual inputs (e.g. see our previous work[20]) are not able to distinguish between two visually similar places. Their combination with an idiothetic system is thus useful: the allothetic information of place cells can be used to recalibrate the grid cell activity in the case of path integration errors, which, in turn, can be used to generate place cells (using a simple supervised Hebbian mechanism as proposed in Ref. [4]), allowing disambiguating two visually similar places. The location of the MEC, upstream of the hippocampus, which is, in turn, an afferent of the entorhinal cortex, provides an anatomical basis for such a modulatory system, suggesting a calibrating role of the hippocampal back-projections to the entorhinal cortex.

Importantly, our model can be used to explain one of the possible advantages of the triangular patterns of grid cells. Indeed, a regular triangular tessellation represents the densest of all possible circle plane packings.[21] Therefore each place cell is associated with a maximum number of grid cells, i.e. all the grid cells that own a grid subfield at the same position as the place field. Consequently, when a path integration error occurs in the grid cell population, the allothetic hippocampal input can very efficiently correct the mismatch, since, as we saw, it projects to a large number of neurons. This ensures very robust-to-noise calibration.

Acknowledgments

This research was supported by the Swiss National Science Foundation (grant nr. 205321-100604 to PFMJ Verschure). The authors thank Reto Wyss for providing the artificial neural networks simulation software *wSim* and Heather Murray for corrections of the manuscript.

References

1. T. Hafting, M. Fyhn, S. Molden, M.-B. Moser and E. I. Moser Microstructure of a spatial map in the entorhinal cortex, *Nature* **436**(7052) (2005) 801–806.
2. M. Fyhn, S. Molden, M. P. Witter, E. I. Moser and M.-B. Moser, Spatial representation in the entorhinal cortex, *Science* **305**(5688) (2004) 1258–1264.
3. F. Sargolini, M. Fyhn, T. Hafting, B. L. McNaughton, M. P. Witter, M.-B. Moser and E. I. Moser, Conjunctive representation of position, direction, and velocity in entorhinal cortex, *Science* **312**(5774) (2006) 758–762.
4. J. O'Keefe and N. Burgess, Dual phase and rate coding in hippocampal place cells: theoretical significance and relationship to entorhinal grid cells, *Hippocampus* **15**(7) (2005) 853–66.
5. K. J. Jeffery and N. Burgess, A metric for the cognitive map: found at last?, *Trends Cogn. Sci.* **10**(1) (2006) 1–3.
6. C. Parron and E. Save, Evidence for entorhinal and parietal cortices involvement in path integration in the rat, *Exp. Brain Res.* **159**(3) (2004) 349–359.
7. J. O'Keefe and J. Dostrovsky, The hippocampus as a spatial map. Preliminary evidence from unit activity in the freely-moving rat, *Brain Res.* **34**(1) (1971) 171–175.
8. V. Braitenberg, *Vehicles, Experiments in Synthetic Psychology*, MIT Press (1984).
9. J. O'Keefeand N. Burgess, Geometric determinants of the place fields of hippocampal neurons, *Nature* **381**(6581) (1996) 425–428.
10. N. Burgess, J. Donnett, K. Jeffery and J. O'Keefe, Robotic and neuronal simulation of the hippocampus and rat navigation, *Philos. Trans. R. Soc. Lond. B. Biol. Sci.* **352**(1360) (1997) 1535–1543.
11. R. Wyss and P. Verschure, Bounded invariance and the formation of place fields, *Adv Neural Inf Process Syst.* S. Thrun, L. Saul and B. Schoelkopf (eds.) **16** (2004).
12. E. Oja, A simplified neuron model as a principal component analyzer, *J. Math. Biol.* **15**(3) (1982) 267–273.
13. S. Haykin, *Neural Networks, a Comprehensive Foundation*, Prentice-Hall (1999).

14. B. McNaughton, C. Barnes, J. Gerrard, K. Gothard, M. Jung, J. Knierim, H. Kudrimoti, Y. Qin, W. Skaggs, M. Suster and K. Weaver, Deciphering the hippocampal polyglot: The hippocampus as a path integration system, *J. Exp. Biol.* **199** (1996) 173–185.
15. A. Samsonovich and B. McNaughton, Path integration and cognitive mapping in a continuous attractor neural network model, *J. Neurosci.* **17**(15) (1997) 5900–5920.
16. S. Stringer, E. Rolls, T. Trappenberg and I. de Araujo, Self-organizing continuous attractor networks and path integration: Two-dimensional models of place cells, *Comput. Neural Syst.* **13**(4) (2002) 429–446.
17. J. Conklin and C. Eliasmith, A controlled attractor network model of path integration in the rat, *J. Comput. Neurosci.* **18**(2) (2005) 183–203.
18. M. C. Fuhs and D. S. Touretzky, A spin glass model of path integration in rat medial entorhinal cortex, *J. Neurosci.* **26**(16) (2006) 4266–4276.
19. A. Guanella and P. Verschure, A model of grid cells based on a path integration mechanism, *Lecture Notes in Computer Science* **4131** (2006) 740–749.
20. R. Wyss, P. König and P. F. M. J. Verschure, A model of the ventral visual system based on temporal stability and local memory, *PLoS Biol.* **4**(5) (2006) 836–843.
21. H. Steinhaus, *Mathematical Snapshots*, 3rd Ed. Dover (1999).